Review

Overview of Operational Global and Regional Ocean Colour Essential Ocean Variables Within the Copernicus Marine Service

Vittorio E. Brando [1,*], Rosalia Santoleri [1], Simone Colella [1], Gianluca Volpe [1], Annalisa Di Cicco [1], Michela Sammartino [1], Luis González Vilas [1], Chiara Lapucci [1], Emanuele Böhm [1], Maria Laura Zoffoli [1], Claudia Cesarini [1], Vega Forneris [1], Flavio La Padula [1], Antoine Mangin [2], Quentin Jutard [2], Marine Bretagnon [2], Philippe Bryère [2], Julien Demaria [2], Ben Calton [3], Jane Netting [3], Shubha Sathyendranath [3], Davide D'Alimonte [4], Tamito Kajiyama [4], Dimitry Van der Zande [5], Quinten Vanhellemont [5], Kerstin Stelzer [6], Martin Böttcher [6] and Carole Lebreton [6]

1   Consiglio Nazionale delle Ricerche, Istituto di Scienze Marine (CNR-ISMAR), 00133 Rome, Italy; rosalia.santoleri@cnr.it (R.S.); simone.colella@cnr.it (S.C.); gianluca.volpe@cnr.it (G.V.); annalisa.dicicco@cnr.it (A.D.C.); michela.sammartino@cnr.it (M.S.); luis.gonzalezvilas@artov.ismar.cnr.it (L.G.V.); chiara.lapucci@cnr.it (C.L.); emanuele.bohm@cnr.it (E.B.); marialaura.zoffoli@cnr.it (M.L.Z.); vega.forneris@cnr.it (V.F.); flavio.lapadula@cnr.it (F.L.P.)
2   ACRI-ST S.A.S., 06904 Sophia-Antipolis, France; antoine.mangin@acri-st.fr (A.M.); quentin.jutard@acri-st.fr (Q.J.); marine.bretagnon@acri-st.fr (M.B.); philippe.bryere@acri-st.fr (P.B.); julien.demaria@acri-st.fr (J.D.)
3   Plymouth Marine Laboratory (PML), Plymouth PL1 3DH, UK; bac@pml.ac.uk (B.C.); jann@pml.ac.uk (J.N.); ssat@pml.ac.uk (S.S.)
4   Aequora, 8200-567 Lisbon, Portugal; davide.dalimonte@aequora.org (D.D.); tamito.kajiyama@aequora.org (T.K.)
5   Royal Belgian Institute of Natural Sciences (RBINS), 1000 Brussels, Belgium; dvanderzande@naturalsciences.be (D.V.d.Z.); qvanhellemont@naturalsciences.be (Q.V.)
6   Brockmann Consult GmbH, 21029 Hamburg, Germany; kerstin.stelzer@brockmann-consult.de (K.S.); martin.boettcher@brockmann-consult.de (M.B.); carole.lebreton@brockmann-consult.de (C.L.)
*   Correspondence: vittorio.brando@cnr.it

Abstract: The Ocean Colour Thematic Assembly Centre (OCTAC) of the Copernicus Marine Service delivers state-of-the-art Ocean Colour core products for both global oceans and European seas, derived from multiple satellite missions. Since 2015, the OCTAC has provided global and regional high-level merged products that offer value-added information not directly available from space agencies. This is achieved by integrating observations from various missions, resulting in homogenized, inter-calibrated datasets with broader spatial coverage than single-sensor data streams. OCTAC enhanced continuously the basin-level accuracy of essential ocean variables (EOVs) across the global ocean and European regional seas, including the Atlantic, Arctic, Baltic, Mediterranean, and Black seas. From 2019 onwards, new EOVs have been introduced, focusing on phytoplankton functional groups, community structure, and primary production. This paper provides an overview of the evolution of the OCTAC catalogue from 2015 to date, evaluates the accuracy of global and regional products, and outlines plans for future product development.

Keywords: Ocean Colour; operational oceanography; essential ocean variables; regional products; sentinel-2; sentinel-3; environmental reporting

1. Introduction

Awareness of the role that the ocean plays in the climate, environment, economy, and more generally the entire society has increased over the past decades [1,2]. At the European level, this has given birth to the Copernicus Marine Environment Monitoring Service (CMEMS), which constitutes one of the six pillar services of the Copernicus program [3]. CMEMS was established in 2015, building on the experience gained through a series of

European projects from 2004 through 2015 (MERSEA, MyOcean, and MyOcean2). Currently, CMEMS is the European provider of operational information (both observations and model outputs) about the global ocean and the European regional seas [4,5].

Within CMEMS, the Ocean Colour Thematic Assembly Centre (OCTAC) provides state-of-the-art Ocean Colour (OC) core products for the global ocean and the European seas based on multiple satellite missions [6–8]. The OCTAC serves users across the scientific and operational oceanography communities, commercial providers focused on the use of marine resources, and public agencies focused on environmental monitoring, with interests in data across oceanic, shelf, and coastal waters. Depending on their applications, these users require different spatial resolutions (i.e., 1 to 4 km in open ocean, 300 m over the shelf, and down to 10s of meters in coastal waters) [9,10]. To meet these needs, the global and regional higher-level combined OCTAC products generate added-value information not readily available from space agencies. Since 2015, the OCTAC has continued to improve the accuracy at the basin level of existing essential ocean variables (EOVs), i.e., chlorophyll-a concentration (CHL), inherent optical properties (IOPs), as well as the radiometry in itself [5,11]. EOVs are key parameters for understanding the spatiotemporal variability of the ocean's physical and biological compartments and are required for inclusion in climate models and projections [11]. Given that the variability in the phytoplankton community structure and the composition of the dissolved and particulate matter occurring across oceanic basins cause significant optical differences [12–14], the regional algorithms differ from those available for global applications because they are specifically derived to reflect the bio-optical characteristics of each European sea [6,13,15]. Blended CHL datasets are produced for all basins applying the appropriate algorithms across the open ocean and coastal waters depending on the water types [6,7,9]. From 2019 onwards, new EOVs related to phytoplankton functional and size groups, community structure, and primary production (PP) were introduced [5,11].

The present review will provide (i) a summary of the operational OC products and datasets across the different spatial resolutions and their evolution from 2015 to date; (ii) an overview of the uncertainty associated with selected variables; (iii) examples of the use of products for operational monitoring and reporting; and (iv) a description of the planned and foreseen product evolutions.

2. Product Overview

Within the CMEMS operational oceanography framework, data are produced both in near-real time (NRT) and as reprocessed multiyear (MY) data delivered as daily consistently projected Level 3 (L3) datasets, as well as monthly average and daily "gap-free" Level 4 (L4) products to overcome cloud cover in subsequent oceanographic analyses [3–5]. The daily L4 datasets are retrieved using optimal interpolation or variants of the DINEOF (data interpolating empirical orthogonal functions) procedure [7,16,17]. The daily NRT products are available by the end of the day following the satellite data acquisition. The daily MY products are produced within 8 to 12 days of acquisition. Since 2015, OCTAC has delivered global and regional OC products covering the CMEMS regions: Global (GLO), Arctic (ARC), and North-East Atlantic (ATL) regions, and Baltic (BAL), Black (BLK), and Mediterranean (MED) seas (Figure 1, Tables 1 and 2).

In 2015, the NRT regional products were based on single-sensors data; between 2016 and 2018, the multisensor datasets were introduced across the whole catalogue (Figure 1). Such datasets are based on harmonized multisensor time series of remote sensing reflectance (R_{rs}) acquired by different OC satellites, significantly increasing the spatial coverage of daily observations) [6,7,9]. These products are available at 1 km spatial resolution for European seas, and at 4 km resolution for the global ocean. Since 2020, the MY processing chains have become fully consistent with the NRT multisensor processors, for all basins. Hence, the only difference between NRT and MY datasets lies in the upstream input data: the Level 2 (L2) granules processed with consolidated auxiliary data (hindcast meteorological and

ephemerides data, usually available a few days after their acquisition) are used to produce the consistent and quality checked MY time series.

In May 2021, higher spatial resolutions were added to the catalogue with the OLCI (Ocean and Land Colour Instrument) datasets at 300 m resolution combining Copernicus Sentinel-3 A and B, as well as the Copernicus Sentinel-2 MSI (MultiSpectral Instrument) datasets at 100 m (Figure 1). The Sentinel 2 MSI datasets are produced for the European coastal waters in a 20 km strip from the coastline, while the OLCI datasets are available at 300 m for all European regional seas and in the global product over a 200 km strip from the coastline (Figure 2). In 2022, the OCTAC catalogue was fully reorganized to reduce the number of products and datasets, so that each product now contains up to five datasets:

(i)   Plankton—with the phytoplankton chlorophyll concentration (CHL), phytoplankton size classes (PSC) and phytoplankton functional types (PFT);

(ii)   Primary Production—integrated productivity within the euphotic zone (PP);

(iii)   Reflectance—with the spectral remote sensing reflectance (R_{rs});

(iv)   Transparency—with the diffuse attenuation coefficient of light at 490 nm (Kd490), Secchi depth (ZSD—an indicator of water transparency), turbidity (TUR), and the suspended particulate matter (SPM);

(v)   Optics—including the inherent optical properties (IOPs), such as absorption and backscattering by particulate and dissolved matter.

As of December 2024, the OCTAC catalogue is composed of 38 OC Products and 214 datasets, across the multisensor, Sentinel-3, and Sentinel-2 data streams (Tables 1 and 2).

The OCTAC operational production is shared among European research centers and private companies to ensure a distribution of the necessary expertise across data streams (Table 2). The development, refinement, and implementation of the processing chains is based on Copernicus funding as well as the uptake of state-of-art algorithms and approaches developed by the space agencies, large collaborative projects, and the OC community.

The OCTAC Catalogue (Tables 1 and 2) includes two complementary global reprocessed products from the Copernicus-GlobColour [7] and OC-CCI (Ocean Colour Climate Change Initiative) [8,9]. These are the main and only two existing operational initiatives providing global long-term daily observations of L3 OC products based on a multisensor approach with 4 km resolution. The Copernicus-GlobColour operational processor ensures consistency of MY and NRT products, with periodical updates when new upstream data from NASA (National Aeronautics and Space Administration) or ESA (European Space Agency)/EUMETSAT (European Organisation for the Exploitation of Meterological Satellites) are available, or following processing chain evolutions [7]. On the other hand, OC-CCI targets climate quality consistency with minimal inter-sensor bias [8,9], with the unavoidable cost of being unable to reach this consistency with an NRT production. Since OC-CCI V5, the CCI algorithms have been applied to delayed-time NRT data to produce interim climate data records (ICDR) for the Copernicus Climate Change Service (C3S) within a month of acquisition, though these should not be considered climate grade. The two products therefore feature different and complementary characteristics, serving various user needs. A downstream service offering NRT products might choose the GC MY to identify anomalies in yesterday's NRT, while a study investigating long-term subtle changes or deriving historical measures for later use may opt for OC-CCI or Copernicus-GlobColour.
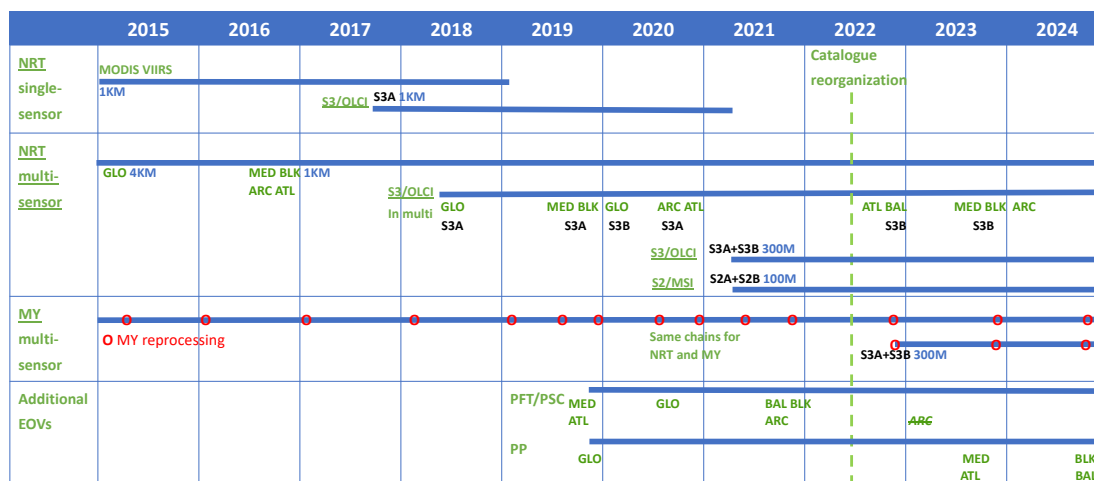
Figure 1. Overview of the OCTAC catalogue evolutions of the single-sensor and multisensor global and regional OC products from 2015 to 2024. The blue lines mark the timelines of each product type; covered basins are marked in green and listed under each line; satellite sensors are marked in black; spatial resolution of products/datasets is marked in blue. The red dots mark the dates of the MY reprocessing.

Table 1. Overview of OCTAC products at various spatial resolutions: 1 and 4 km multisensor datasets, merged Sentinel-3 OLCI A + B datasets at 4 km and 300 m, and merged Sentinel-2 MSI A + B datasets at 100 m.

CMEMS Region	Multi-Sensor 1 km (Regions), 4 km (ARC, GLO)				Sentinel-3 OLCI A + B 300 m (Regions and GLO)/4 km (GLO)				Sentinel-2 MSI A + B 100 m			
	NRT		MY		NRT		MY		NRT		MY	
	L3	L4	L3	L4	L3	L4	L3	L4	L3	L4	L3	L4
Arctic Ocean	-	-	✓	✓	✓	✓	✓	✓	✓	✓	-	-
NE Atlantic Ocean	✓	✓	✓	✓	✓	-	✓	-	✓*	✓*	-	-
Baltic Sea	-	-	✓	✓	✓	✓	✓	✓	✓	✓	-	-
Black Sea	✓	✓	✓	✓	✓	✓	✓	✓	✓	✓	-	-
Mediterranean Sea	✓	✓	✓	✓	✓	✓	✓	✓	✓	✓	-	-
Global	✓	✓	✓	✓	✓	✓	✓	✓	-	-	-	-
Global (C3S/OC-CCI)			✓	✓								

* Due to size of the files, the Sentinel-2 based products for the North-East Atlantic are produced over the Iberia–Biscay–Ireland (IBI) and North-West Shelf (NWS) areas and are provided in tiles linked to UTM zones.

Table 2. Listing of the OCTAC products in December 2024.

Region	L3/L4	NRT/MY	Product Name	DOI	Production Unit
GLO	L3	NRT	OCEANCOLOUR_GLO_BGC_L3_NRT_009_101	https://doi.org/10.48670/moi-00278	ACRI-ST
GLO	L4	NRT	OCEANCOLOUR_GLO_BGC_L4_NRT_009_102	https://doi.org/10.48670/moi-00279	ACRI-ST
GLO	L3	MY	OCEANCOLOUR_GLO_BGC_L3_MY_009_103	https://doi.org/10.48670/moi-00280	ACRI-ST
GLO	L4	MY	OCEANCOLOUR_GLO_BGC_L4_MY_009_104	https://doi.org/10.48670/moi-00281	ACRI-ST
GLO	L3	MY	OCEANCOLOUR_GLO_BGC_L3_MY_009_107	https://doi.org/10.48670/moi-00282	BC/PML *
GLO	L4	MY	OCEANCOLOUR_GLO_BGC_L4_MY_009_108	https://doi.org/10.48670/moi-00283	BC/PML *
ATL	L3	NRT	OCEANCOLOUR_ATL_BGC_L3_NRT_009_111	https://doi.org/10.48670/moi-00284	ACRI-ST
ATL	L3	MY	OCEANCOLOUR_ATL_BGC_L3_MY_009_113	https://doi.org/10.48670/moi-00286	ACRI-ST

Table 2. *Cont.*

| Region	L3/L4	NRT/MY	Product Name	DOI	Production Unit
ATL	L4	NRT	OCEANCOLOUR_ATL_BGC_L4_NRT_009_116	https://doi.org/10.48670/moi-00288	ACRI-ST
ATL	L4	MY	OCEANCOLOUR_ATL_BGC_L4_MY_009_118	https://doi.org/10.48670/moi-00289	ACRI-ST
ARC	L3	NRT	OCEANCOLOUR_ARC_BGC_L3_NRT_009_121	https://doi.org/10.48670/moi-00290	CNR
ARC	L4	NRT	OCEANCOLOUR_ARC_BGC_L4_NRT_009_122	https://doi.org/10.48670/moi-00291	CNR
ARC	L3	MY	OCEANCOLOUR_ARC_BGC_L3_MY_009_123	https://doi.org/10.48670/moi-00292	CNR
ARC	L4	MY	OCEANCOLOUR_ARC_BGC_L4_MY_009_124	https://doi.org/10.48670/moi-00293	CNR
BAL	L3	NRT	OCEANCOLOUR_BAL_BGC_L3_NRT_009_131	https://doi.org/10.48670/moi-00294	CNR
BAL	L4	NRT	OCEANCOLOUR_BAL_BGC_L4_NRT_009_132	https://doi.org/10.48670/moi-00295	CNR
BAL	L3	MY	OCEANCOLOUR_BAL_BGC_L3_MY_009_133	https://doi.org/10.48670/moi-00296	CNR
BAL	L4	MY	OCEANCOLOUR_BAL_BGC_L4_MY_009_134	https://doi.org/10.48670/moi-00308	CNR
MED	L3	NRT	OCEANCOLOUR_MED_BGC_L3_NRT_009_141	https://doi.org/10.48670/moi-00297	CNR
MED	L4	NRT	OCEANCOLOUR_MED_BGC_L4_NRT_009_142	https://doi.org/10.48670/moi-00298	CNR
MED	L3	MY	OCEANCOLOUR_MED_BGC_L3_MY_009_143	https://doi.org/10.48670/moi-00299	CNR
MED	L4	MY	OCEANCOLOUR_MED_BGC_L4_MY_009_144	https://doi.org/10.48670/moi-00300	CNR
BLK	L3	NRT	OCEANCOLOUR_BLK_BGC_L3_NRT_009_151	https://doi.org/10.48670/moi-00301	CNR
BLK	L4	NRT	OCEANCOLOUR_BLK_BGC_L4_NRT_009_152	https://doi.org/10.48670/moi-00302	CNR
BLK	L3	MY	OCEANCOLOUR_BLK_BGC_L3_MY_009_153	https://doi.org/10.48670/moi-00303	CNR
BLK	L4	MY	OCEANCOLOUR_BLK_BGC_L4_MY_009_154	https://doi.org/10.48670/moi-00304	CNR
ARC	L3	NRT	OCEANCOLOUR_ARC_BGC_HR_L3_NRT_009_201	https://doi.org/10.48670/moi-00061	BC-RBINS
BAL	L3	NRT	OCEANCOLOUR_BAL_BGC_HR_L3_NRT_009_202	https://doi.org/10.48670/moi-00079	BC-RBINS
NWS	L3	NRT	OCEANCOLOUR_NWS_BGC_HR_L3_NRT_009_203	https://doi.org/10.48670/moi-00118	BC-RBINS
IBI	L3	NRT	OCEANCOLOUR_IBI_BGC_HR_L3_NRT_009_204	https://doi.org/10.48670/moi-00107	BC-RBINS
MED	L3	NRT	OCEANCOLOUR_MED_BGC_HR_L3_NRT_009_205	https://doi.org/10.48670/moi-00109	BC-RBINS
BLK	L3	NRT	OCEANCOLOUR_BLK_BGC_HR_L3_NRT_009_206	https://doi.org/10.48670/moi-00086	BC-RBINS
ARC	L4	NRT	OCEANCOLOUR_ARC_BGC_HR_L4_NRT_009_207	https://doi.org/10.48670/moi-00062	BC-RBINS
BAL	L4	NRT	OCEANCOLOUR_BAL_BGC_HR_L4_NRT_009_208	https://doi.org/10.48670/moi-00080	BC-RBINS
NWS	L4	NRT	OCEANCOLOUR_NWS_BGC_HR_L4_NRT_009_209	https://doi.org/10.48670/moi-00119	BC-RBINS
IBI	L4	NRT	OCEANCOLOUR_IBI_BGC_HR_L4_NRT_009_210	https://doi.org/10.48670/moi-00108	BC-RBINS
MED	L4	NRT	OCEANCOLOUR_MED_BGC_HR_L4_NRT_009_211	https://doi.org/10.48670/moi-00110	BC-RBINS
BLK	L4	NRT	OCEANCOLOUR_BLK_BGC_HR_L4_NRT_009_212	https://doi.org/10.48670/moi-00087	BC-RBINS

* Global ocean OC-CCI reprocessed multisensor data produced by PML (2015–2023) and by BC in 2023–2025.

2.1. Upstream OC Data Streams

Over the years, the upstream data shifted from OC science missions—i.e., SeaWiFS (Sea-viewing Wide Field-of-view Sensor), MERIS (MEdium Resolution Imaging Spectrometer) and MODIS (Moderate Resolution Imaging Spectroradiometer)—towards operational missions (Figure 3). As well as the two OLCIs on the Copernicus Sentinel-3 A and B and three VIIRSs (Visible Infrared Imaging Radiometer Suites) on NOAA's (National Oceanic and Atmospheric Administration) SNPP (Suomi-national polar-orbiting partnership), NOAA-20 and NOAA-21, the two MSI (MultiSpectral Instrument) sensors on the Copernicus Sentinel-2 A and B satellite are ingested for the coastal products due to their finer spatial resolution, although they were initially designed for terrestrial applications and have a revisit time of 3–5 days (Figure 3). In 2015, all NRT regional products were based on MODIS and VIIRS; between 2016 and 2018 these datasets were then replaced by multisensor datasets [6,7,9] (Figure 1). The number of sensors contributing to the multisensor product time series changed over the years from one sensor (SeaWiFS) from 1997 to 2002, up to six sensors (MODIS-Aqua, VIIRS-SNPP/NOAA-20/NOAA-21, and OLCI-Sentinel-3A/B) from late 2022 to the moment of writing (Figure 3).

(A)

(B)
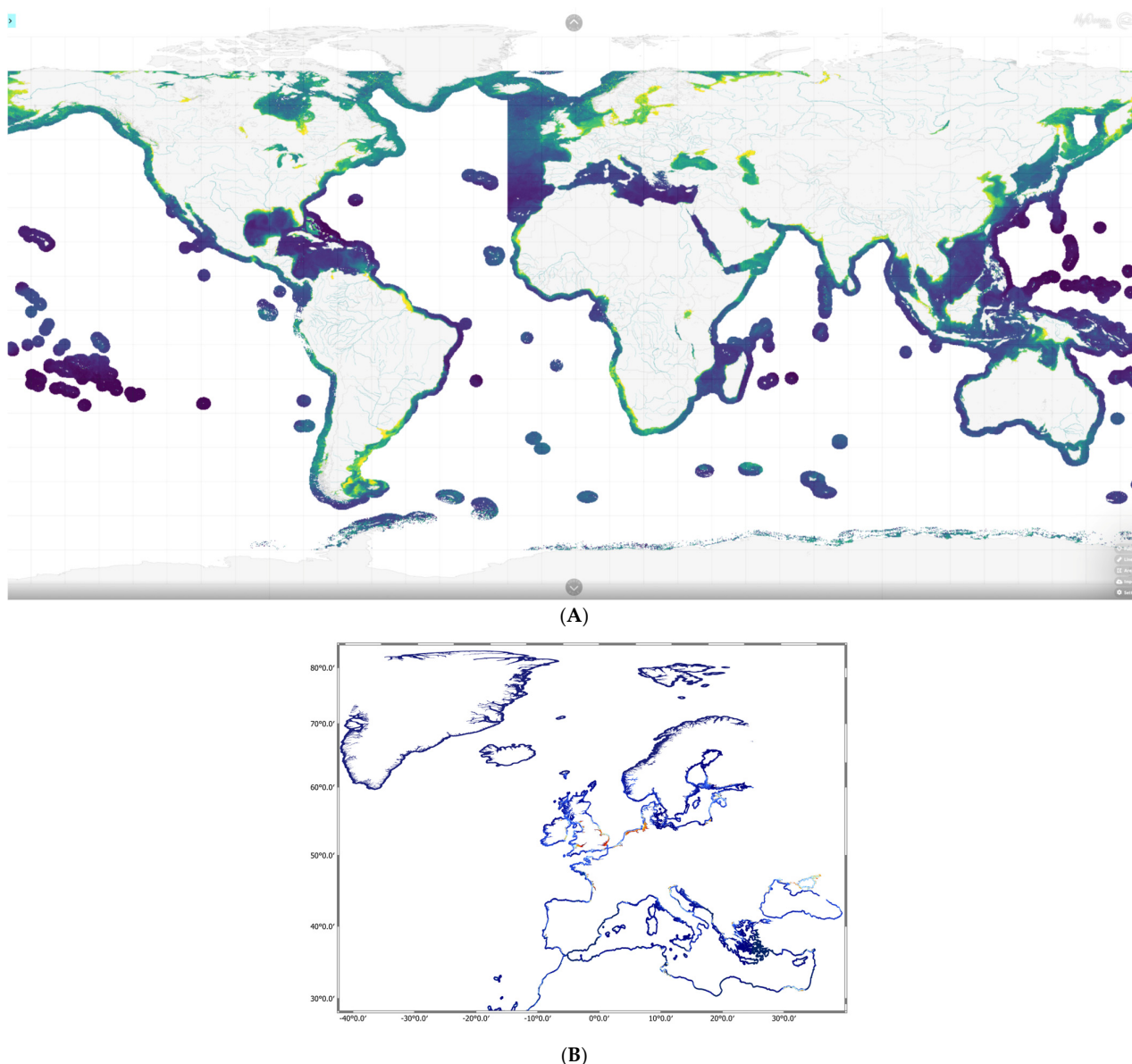
Figure 2. Spatial coverage of the Sentinel-3 OLCI 300 m and Sentinel-2 MSI 100 m datasets. (**A**) All European regional seas and a 200 km strip from the coastline in the global product for Sentinel-3 OLCI. (**B**) A 20 km strip from the coastline for the European coastal waters covered in 5 days with Sentinel-2 MSI.

2.2. Merging Strategies and Atmospheric Correction

Within OCTAC, specific strategies to merge data from sensors with different sets of central wavelengths and spectral response functions are adopted in the processing chains. For the OC-CCI multisensor production, atmospheric correction is performed independently for each sensor, and the merging is performed for the calibrated reflectances, after band shifting to the reference sensor bands [8,9,18,19]. In particular, MERIS, MODIS, VIIRS, and OLCI data were processed to L2 with the POLYMER algorithm [20,21] while L2 data downloaded from NASA were used for SeaWiFS. For the Mediterranean and Black Sea regional products, the method developed within OC-CCI has been adapted to rely on L2 data distributed by space agencies [6]. The Copernicus-GlobColour products for GLO and ATL are based on the L2 data distributed by the agencies with multisensor merging and flagging strategies detailed in Garnesson et al. [7].
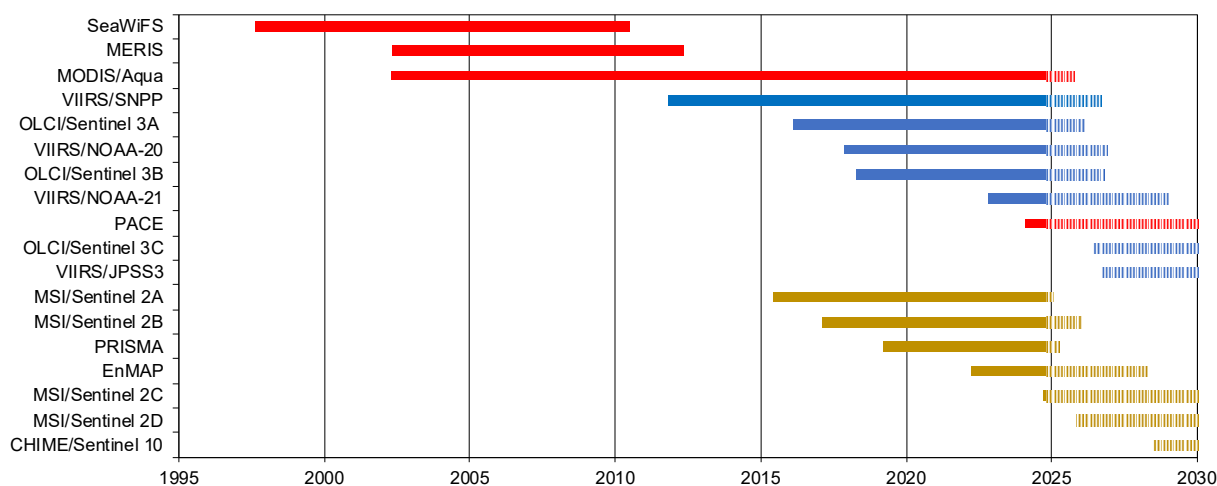
Figure 3. OC sensors and high-resolution imagers adopted upstream in OCTAC processing chains. Timelines of legacy, and current and forthcoming (approved and planned) sensors are displayed (source CEOS): red identifies science OC missions, blue identifies operational OC missions, and brown identifies high-resolution/land imagers.

Combining Sentinel-3 A and B (Sentinel-3 OLCI datasets), as well as combining Sentinel-2 A and B (Sentinel-2 MSI datasets), does not require band-shifting or inter-sensor bias correction because the two companion A and B sensors are assumed to be fully consistent. The Sentinel-3 OLCI datasets for the global and regional products are based on L2 reflectances distributed by EUMETSAT [22], except for the Baltic Sea, where the EUMETSAT L2 processor often yields inaccurate R_{rs} spectra with low and even negative values [23–25]. Thus for the atmospheric correction of the OLCI L1 granules in the Baltic Sea, the OLCI neural network swarm [26] was used until 2023, and then POLYMER [20,21] was selected based on a round-robin comparison of several algorithms [25].

The Sentinel-2 MSI products are available every 3–5 days at each location for a 20 km strip from the coastline of the European coasts, characterized by diverse atmospheric conditions and fast-changing water types in space and time (Figure 2B). As an operational L2 reflectance product for water applications is not available within Copernicus for Sentinel-2 MSI [27], two algorithms, C2RCC (version 1.0, normal NN) [28,29] and ACOLITE/DSF [30], are used as the baseline atmospheric correction approach to deal with both optically complex and clear waters under the very challenging atmospheric conditions of the nearshore environments [31]. These two methods are highly complementary because ACOLITE/DSF makes no assumption about the water reflectance, thus achieving good results even for unexpected water types (e.g., dredging plumes, very concentrated algal blooms, etc.). Instead, C2RCC constrains the water reflectance to correspond to the training data, always retrieving R_{rs} spectra that look like water. This extra information/constraint on water reflectance, embedded within the C2RCC approach, provides greater retrieval power in the most challenging circumstances (sunglint, highly absorbing waters) but at the expense of imposing a solution for R_{rs} that may not correspond to reality. The C2RCC to ACOLITE/DSF pixel-based switching is performed by means of the comparison of the R_{rs} (560) and R_{rs} (865) spectral bands (as provided by the C2RCC processor).

2.3. Retrieval Algorithms in the Global and Regional Processing Chains

2.3.1. Chlorophyll Algorithms

This section provides an overview of the CHL algorithms implemented in the operational processing chains for the global and regional products across the three spatial resolutions. All processing chains generate blended CHL datasets by ensuring that the most appropriate algorithms are applied across the water types that occur in the open ocean and coastal waters. The selection of the algorithms for CHL retrieval and the merging

schemes were carried out based on the optical characteristics of each basin and round-robin procedures. To generate the NRT and MY CHL for the OLCI and the multisensor datasets, the regional bio-optical algorithms are consistently applied for each basin. For the S2 MSI datasets, the same processing chain is applied across all European waters to generate NRT CHL.

For the Global Ocean, CHL concentration estimated within the Copernicus-GlobColour as a daily multisensor merged dataset, where CHL values are individually computed for each sensor using a blended algorithm and then combined [7]. For oligotrophic waters, the product relies on the CI algorithm [32], while for mesotrophic and coastal waters the OC5 algorithm [33] was tuned for each sensor. The OC5 and CI blending uses the same approach as NASA's implementation of the CI algorithm [32], with a transition between 0.15 to 0.2 mg m^{-3} to ensure a smooth merging.

For the Global Ocean, the CHL values for the OC-CCI products are calculated by blending algorithms based on the water-types utilising the same OC-CCI R_{rs} described above [8,9]. For v6.0, the blending of the OCI algorithm (as implemented by NASA, itself a combination of CI and OC4 [32]), the OCI2 algorithm (an updated OCI parameterization), the OC2 algorithm and the OCx algorithm [8,19].

For the Arctic and Atlantic Oceans, the regional CHL algorithm adopted until 2022 was OC5CCI—i.e., a variation of OC5 [33]—developed by IFREMER and PML [34]. To this end, an OC5CCI look-up table was specifically generated for application over OC-CCI daily merged R_{rs}. The resulting OC5CCI algorithm was tested and selected after a calibration exercise and sensibility analysis of the existing algorithms (OC3, OC4, OCI, OC5CI, OC5, OC5CCI) that included a round-robin quantitative performance assessment against in situ data [34]. Following a catalogue reorganization and change of production responsibility, since 2023 the Atlantic Ocean product has been retrieved with the Copernicus-GlobColour processor described above [7], while for the Arctic a new regional algorithm was developed [35], and applied to OLCI and OC-CCI R_{rs}.

The water-column in the Arctic region has particular characteristics, namely high and heterogeneous distribution of colored dissolved organic matter (CDOM) due to freshwater inputs that reach different ARC sectors, which limits the performance of global CHL algorithms [36,37]. When acquiring satellite data in polar regions, additional challenges arise due to low solar zenith angles, frequent ice coverage and high aerosol content [37] that usually introduce high uncertainties in retrieving water-leaving radiance. Since 2023, CHL has been retrieved by a new regional algorithm, seasonal spatially adjusted for the Arctic Ocean (CHL-SeSARC) [35], developed using supervised machine learning techniques and trained with a compilation of in situ databases for the Arctic waters from 1998 to 2018. In the proposed pan-Arctic CHL algorithm, the use of the longitude of the pixel center and the day of the year enables accounting for the regional particularities and spatial heterogeneity within the ARC and the seasonal variability of the bulk phytoplankton community and/or the associated uncertainties in atmospheric correction.

In the Mediterranean Sea, the blended CHL product is based on two regional algorithms: the MedOC4, an updated version of the regionally parameterized maximum band ratio [6] for clear waters, and the ADOC4 algorithm [38] for optically complex waters. From 2020, the determination of the water type accounts specifically for waters with high CHL concentration due to phytoplankton blooms (e.g., Gulf of Lions) or mixing (e.g., Alborán Sea) that can be erroneously identified as Case II waters [39].

In the Black Sea, the retrieval of the CHL concentration is based on a merging scheme [40] designed for two different regional algorithms exhibiting lower and higher optical complexity. These are, respectively, a band-ratio algorithm based on two wavelengths (490 and 555 nm) [41], and a multilayer perceptron (MLP) neural net based on R_{rs} values at three wavelengths (490, 510, and 555 nm) that features interpolation capabilities helpful to fit data non-linearities [40]. In 2019, this merging scheme substituted the regional band ratio approach by Kopelevich et al. [42].

In the Baltic Sea, CHL is derived from the MLP neural net developed under the umbrella of the BiOMaP program of JRC/EC [15,43,44]. The BAL product is based on an ensemble algorithm that combines the CHL retrievals from individual MLPs based on different R_{rs} spectral subsets to address the optical complexity of the basin and to account for the temporal and spatial variation of uncertainties introduced by the atmospheric correction [25,45]. In 2020, this ensemble approach substituted the previous operational regional algorithm based on the recalibration of the OC4v6 with in situ data [46].

The coastal products based on Sentinel 2 MSI introduced in 2021 are produced for a 20 km strip from the coastline in the coastal waters of the ARC, NWS, BAL, IBI, MED, and BLK regions (Figure 2B). For these products, the same processing chain is applied across all European waters to address the fast-changing water types in space and time by combining different algorithms for the CHL concentration retrieval. The CHL datasets are generated by merging two complementary algorithms following the approach of Lavigne et al. [47]: the OC3 empirical blue-green bands ratio algorithm [48], and the Gons [49,50] semi-analytical algorithm. The OC3 algorithm was selected for application over low-to-moderate biomass waters and over clear-to-moderately turbid waters. The Gons algorithm was chosen for application over moderate-to-high-biomass waters and for turbid coastal waters. The operational limits of the CHL algorithms are determined on the basis of the optical conditions of the considered pixels, using the quality control routines developed by Lavigne et al. [47] adapted to the Sentinel-2 bands. Within this framework, pixels are flagged in waters with a turbidity level of approximately 10 FNU or higher and CHL lower than 5 mg m^{-3}, because the uncertainties associated with CHL retrieval in such water types would be too high.

2.3.2. Phytoplankton Type Variables

The phytoplankton type variables were introduced in the OCTAC catalogue from 2019 for the global ocean and all regional seas using global and regionally tuned methods [39,51–56]. The phytoplankton size classes (PSCs) and phytoplankton functional types (PFTs) are expressed as CHL concentration (mg m^{-3}). Both for the global ocean and regional seas, PFTs include diatoms, dinoflagellates, green algae, prokaryotes, and haptophytes (except for BAL). For GLO and ATL, the prochlorococcus group is also distributed, while cryptophytes are provided only for MED and BAL. PSCs consist of three main size groups, micro-, nano- and pico-phytoplankton, based on Sieburth et al.'s [57] size classification and Vidussi et al.'s [58] approach founded on the relationships between diagnostic pigments, taxonomic groups, and their most common dimensions. For BLK, only PSCs are distributed.

For both algorithm calibration and validation, the in situ Chl-a concentration of each group was quantified through diagnostic pigment analysis (DPA) [58] and its implementations and refinements [51,59–61]. The DPA was updated for GLO and ATL [54,55], and regionalized for MED, BAL, and BLK [39,53,56]. For GLO and ATL, the algorithm [49,50] was initially implemented using OLCI reflectance in the visible spectrum (bands comprised between 400 and 681 nm) using an empirical orthogonal function (EOF) approach and then extended to the multisensor datasets. The regional algorithms for PFT and PSC retrieval for MED, BAL, and BLK [39,53,56] rely on empirical functions based on statistical relationships between the in situ contribution of each group (PFT or PSC) and the corresponding log10-transformed in situ CHL concentrations (that are applied to each of the regional CHL datasets).

2.3.3. Inherent Optical Properties

The operational processing chains for the global and regional products across the three spatial resolutions have implemented different approaches for retrieval of the main IOPs. The coefficients for the absorption by phytoplankton (aph), the absorption by dissolved and detrital matter (adg), and the backscattering by particulate matter (bbp) are provided at reference wavelengths.

For MED, BLK, BAL, and ARC multisensor and OLCI datasets, the algorithm used to produce the aph(443), adg(443), and bbp(443) is the quasi-analytical algorithm (QAA V6 [62,63]), also used in the context of the band-shifting procedures [18]. For all the Sentinel 2 MSI products for European coastal waters, the bbp coefficient is spectrally dependent and is also estimated using the QAA V6 [62,63].

For GLO and ATL since 2023, the adg(443) and bbp(443) are estimated from a semi-analytical model based on Kd490 and R$_{rs}$ [64,65], replacing the retrieval carried out with the Garver–Siegel–Maritorena (GSM01) bio-optical model [66] implemented in the Copernicus-GlobColour processor described above [7].

2.3.4. Primary Production

Primary Production data products were added to the catalogue in 2019. As of the December 2024 version, PP is distributed for the GLO, ATL, MED, BLK, and BAL (Figure 1). The GLO and ATL version is based on the Antoine and Morel algorithm [67], and uses OC products—merged CHL, PAR (photosynthetically active radiation [68]), sea surface temperature from OSTIA (operational sea surface temperature and ice analysis) and mixed layer depth from model reanalysis (GLORYS12V1) [69]).

The regional PP datasets for MED, BLK, and BAL are based on an updated version of the bio-optical model by Morel [70], incorporating the regional CHL retrievals [39]. This model uses outputs from the atmospheric model by Tanré et al. [71], which allows the estimation of the photosynthetic radiation at the sea surface and its attenuation through the water column. With a parameterization of the main physiology processes, the model allows the computation of the primary productivity starting from algal biomass concentration. The empirical approach developed by Morel and Berthon [72] establishes relationships between the pigment concentration in the upper layer, the integrated content across the entire euphotic zone, and the shape of the vertical pigment profile. As a result, this model enables the linkage of satellite-derived pigment concentrations with vertical pigment distributions. For the regional products, the atmospheric model was replaced by the revised version of the multispectral ocean atmosphere spectral irradiance model (OASIM [73]). This updated OASIM model provides daily estimations of the direct and diffuse irradiance over the ocean with 5 nm spectral resolution (400–700 nm) and 4 km spatial resolution. Moreover, the empirical approach by Morel and Berthon [72] to associate a pigment vertical distribution with a satellite pigment concentration has been refined for MED through the specific utilization of a Mediterranean Sea in situ dataset (MedBiOp, [6]).

3. Uncertainty of OCTAC Products

The validation of the satellite products is carried out by pairwise comparison against in situ reference observations using a common methodology defined and agreed within CMEMS [74]. Since those distributed by OCTAC are all multisensor daily products, the temporal collocation criteria are more relaxed than those of the L2 matchup analyses (e.g., [75]) and allow the inclusion of any in situ observations up to 24 h. As for the spatial matching, the median values are extracted from a $n \times n$ satellite data pixels (with n varying according to the product spatial resolution), centered on the in situ measurement location only in the presence of at least 50% valid values and a coefficient of variation smaller than 20% [75]. The quality assessment is mainly based on an inter-comparison with in situ data gathered from publicly available datasets (e.g., [76]) and/or collected from the production units (e.g., MedBiOp, [6]). MY and NRT are considered together as a homogeneous time series for the assessment. Many uncertainties are linked to these in situ data (e.g., instruments quality, methodologies, water depth of sample compared to surface satellite observation, and time of observations [74,75]). Hence, the estimated accuracy numbers (EANs [74]) used to compare satellite and in situ observations (Table 3) are based on a regression of type 2 (with a reasonable assumption of the same weight for observation and in situ) to compute the determination coefficient (r^2), slope, and intercept

(S, I) and completed by the root mean square distance (RMSD), the center-pattern root mean square distance (cRMSD), and the bias.

The validation metrics for all datasets for the OCTAC products are reported in quality information documents (QuIDs) that are updated with every operational release. The QuIDs for all products can be retrieved from the CMEMS portal following the links reported in Table 2.

Table 3. Metrics used to compare the estimated (satellite-based) dataset $X^E_{i,i=1.N}$ to a reference (in situ) dataset $X^M_{i,i=1.N}$. For log-normally distributed variables (such as Chl), both datasets are log-transformed prior to computing the metrics.

Name	Definition
Estimated dataset mean ($\overline{X}^E$)	$\overline{X}^E = \frac{1}{N}\sum_{i=1}^{N} X^E_i$
Reference dataset mean ($\overline{X}^M$)	$\overline{X}^M = \frac{1}{N}\sum_{i=1}^{N} X^M_i$
Type-2 slope (S)	$S = \dfrac{\sum_{i=1}^{N}\left(X^E_i-\overline{X}^E\right)^2 - \sum_{i=1}^{N}\left(X^M_i-\overline{X}^M\right)^2 + \left[\left\{\sum_{i=1}^{N}\left(X^E_i-\overline{X}^E\right)^2 - \sum_{i=1}^{N}\left(X^M_i-\overline{X}^M\right)^2\right\}^2 + 4\left\{\sum_{i=k}^{N}\left(X^E_k-\overline{X}^E\right)\left(X^M_k-\overline{X}^M\right)\right\}^2\right]^{\frac{1}{2}}}{2\sum_{i=k}^{N}\left(X^E_k-\overline{X}^E\right)\left(X^M_k-\overline{X}^M\right)}$
Type-2 intercept (I)	$I = \overline{X}^E - S\cdot\overline{X}^M$
Determination coefficient (r^2)	$r^2 = \dfrac{\left[\sum_{i=1}^{N}\left(X^E_i-\overline{X}^E\right)\left(X^M_i-\overline{X}^M\right)\right]^2}{\sum_{i=1}^{N}\left(X^E_i-\overline{X}^E\right)^2 \sum_{i=1}^{N}\left(X^M_i-\overline{X}^M\right)^2}$
Root mean square difference (RMSD)	$RMSD = \sqrt{\dfrac{\sum_{i=1}^{N}\left(X^E_i-X^M_i\right)^2}{N}}$
Center-pattern root mean square difference (cRMSD)	$cRMSD = \sqrt{\dfrac{\sum_{i=1}^{N}\left\{\left[X^E_i-\left(\sum_{j=1}^{N} X^E_j\right)\right]-\left[X^M_i-\left(\sum_{k=1}^{N} X^M_k\right)\right]\right\}^2}{N}}$

Uncertainty Associated to Chlorophyll Datasets

As an example of the OCTAC validation effort, Table 4 provides a summary of the matchup metrics for all CHL datasets for the global and regional products across the three spatial resolutions. For GLO and ATL, the EANs values show a good relationship between in situ HPLC measurements (from 1997 to present) and CHL retrieved with the GlobColour approach [7]). For daily, the statistics show a good correlation: r^2 of 0.75 (0.74 at the Atlantic level) associated to an optimal regression line 1:1 (0.94 on the Atlantic).

These statistics, based on several thousands of in situ observations covering both coastal and clear ocean, demonstrate the quality of this product for many applications. The interpolated product shows a slight degradation but r^2 still reaches 0.71, meaning that it is also of applicative interest, for instance, for model assimilation purposes. The Atlantic interpolated product at 1 km shows a similar r^2 of 0.72. The OLCI specific EANs suffer from a very limited number of matchups and should improve over time. The r^2 is good at more than 0.7, but the slope is high because of a slight overestimation at higher values.

For the OC-CCI global product [8,9,19], the CHL results show a strong correlation (r^2 = 0.88) with low error (RMSD = 0.23 and cRMSD = 0.23) and low bias (−0.022) for more than 30,000 matched in situ observations. Based on the high quality of the product, and in particular the very low bias, the OC-CCI CHL product is within the GCOS target requirement of 5% accuracy, thus suggesting that the OC-CCI program is meeting the GCOS target for the ECV climate quality criteria.

For MED, the CHL validation of the multisensor datasets show good relationships between in situ measurements and CHL retrieval with the regional algorithm [6], although for in situ values larger than 0.3 mg m^{-3} there is a slight dispersion increase. The EANs show low biases (i.e., 0.0017 and −0.029 for daily and daily-interpolated, respectively, Table 3) with r^2 values of 0.79 and 0.78 for daily and daily-interpolated, respectively.

Table 4. Summary of the OCTAC validation metrics for CHL datasets. All symbols are defined in Table 3.

Region	CHL Dataset	N	Slope	Intercept	r^2	RMSD	cRMSD	Bias
GLO (GC)	MULTI MY L3 daily 4 km	17,019	1.00	0.05	0.75	0.340	0.340	0.050
	MULTI MY L4 interpolated 4 km	36,438	0.99	0.00	0.71	0.370	0.370	0.010
	OLCI MY L3 4 km	669	1.32	0.21	0.68	0.395	0.388	0.078
	OLCI MY L3 300 m	288	1.35	0.27	0.71	0.417	0.376	0.180
GLO (OC-CCI)	MULTI MY L3 daily 4 km	34,221	0.925	−0.026	0.88	0.226	0.225	−0.022
ATL	MULTI MY L3 daily 4 km	4621	0.94	0.07	0.74	0.350	0.34	0.080
	MULTI MY L4 interpolated 4 km	10,397	0.94	0.04	0.72	0.360	0.36	0.050
	OLCI MY L3 1 km	72	1.21	0.14	0.83	0.261	0.25	0.073
	OLCI MY L3 300 m	35	1.54	0.24	0.78	0.324	0.281	0.161
ARC	MULTI MY L3 4 km	323	0.67	−0.04	0.68	0.268	0.267	0.015
	OLCI MY L3 300 m	21	0.64	0.06	0.75	0.215	0.193	0.641
BAL	MULTI MY L3 1 km	2070	1.09	−0.21	0.31	0.375	0.335	−0.168
	OLCI MY L3 300 m	460	0.83	0.01	0.32	0.271	0.262	−0.071
BLK	MULTI MY L3 1 km	1154	0.63	0.09	0.28	0.480	0.367	0.042
MED	MULTI MY daily L3 1 km	742	0.97	−0.02	0.79	0.250	0.250	0.002
	MULTI MY L4 interpolated 1 km	1819	0.91	−0.11	0.78	0.258	0.256	−0.029
	MULTI MY L4 interpolated-only 1 km	1084	0.87	−0.16	0.78	0.263	0.259	−0.050
All zones	MSI NRT daily 100 m	700	0.90	0.26	0.48	0.549	0.492	0.257
BAL	MSI NRT daily100 m	188	0.86	0.15	0.22	0.478	0.471	0.085
NWS	MSI NRT daily 100 m	289	1.03	0.22	0.12	0.557	0.508	0.245
IBI	MSI NRT daily 100 m	120	0.94	0.40	0.03	0.582	0.432	0.374
MED	MSI NRT daily 100 m	103	1.15	0.54	0.64	0.608	0.446	0.341

For BLK, the performances of the daily CHL retrieved with the regional merging scheme [40] yield a r^2 = 0.39 and a bias = 0.17 due to the extremely complex waters of the basin and the limited number of matchups. With interpolated data, the correlation is worse (r^2 = 0.28), but the bias is better (0.042). Dispersion of the data is evident for the entire CHL range [39].

For BAL, in view of its optical complexity, the matchup window is limited to 6 h [25,45]. The assessment of the CHL retrieved with the regional ensemble approach [25,45] shows an r^2 of 0.312 and RPD and APD of −2.8 and 66.1% for the MY multisensor datasets and an r^2 of 0.324 and RPD and APD of 4 and 51.2% for the NRT ad MY OLCI 300 m datasets. The EANs for the OLCI results are consistent with the MY multisensor datasets even with a lower number of matchups available from 2016 to date (460 vs. 2070). These matchup statistics may appear unsatisfactory, but represent an adequate performance for the CDOM-dominated optically complex waters of the Baltic Sea and an improvement of those reported in [25,45] based on a more limited in situ dataset.

The validation of CHL retrieval for ARC based on the new machine learning pan-Arctic regional algorithm [35] shows an r^2 of 0.681 and a RMSD of 0.268 for the MY multisensor datasets and an r^2 of 0.75 and RMSD of 0.215 for the NRT and MY OLCI 300 m datasets. The OLCI results should be interpreted with caution as they may be influenced by the lower number of matchups (21 vs. 323) and presented only to provide a preliminary indication of performance.

For the validation of the CHL datasets in the HROC coastal products based on the merging approach developed for European waters [47–50], the matchups between satellite and in situ observations when assessed over four regions together (BAL, NWS, IBI, MED), follow the 1:1 line (slope = 0.90) with a slight overestimation across the range <1 to 10 mg m^{-3}. A wider dispersion of points is observed (r^2 = 0.48), which can be expected because of the use of the broad spectral bands particularly in the blue region (443 nm and

490 nm) for CHL estimation. Additionally, the median time difference of 70 min between in situ and satellite measurements in dynamic coastal zones also contributes to the higher dispersion. For each of the four single regions (i.e., BAL, NWS, IBI, MED) the matchup statistics are based on a limited number of observations. Furthermore, it should be noted that matchup results for CHL in the ARC and BLK region are not present in this matchup analysis due to the scarcity of suitable in situ records available from 2020 onwards; hence these datasets are released for community evaluation.

## 4. Contributions to Environmental Reporting

Within CMEMS, OCTAC also contributes to ocean monitoring through the distribution of specific operational indicators delivering information on the state, variability, and change of CHL for all regions. To ensure state-of-the-art ocean monitoring in real time, the ocean monitoring indicator (OMI) framework requires that the indicator time series, their visualization, a description, and additional documents such as product and quality information are updated regularly in an operational mode [5]. As an illustration of the contributions to operational ocean monitoring, Figure 4 presents the Mediterranean Sea CHL trend analysis, derived from two operational OMIs (1997–2023) of satellite CHL based on the CMEMS L4 product.

The trend analysis (Figure 4A) shows that the basin is undergoing a general biomass decrease, in particular starting from 2011. Surface ocean warming [77,78] translates into stronger thermal stratification of the water column for increasingly extended periods. In turn, this implies a progressive nutrient decline into the upper mixed layer, which likely forces the phytoplankton vertical distribution with a deep CHL maximum (DCM) persisting in recent years for longer periods than ever before. From the remote sensing point of view, this has the effect of reducing the phytoplankton biomass resident time in the upper layer where the satellite sensors can effectively observe them. Therefore, the trend of $-0.73 \pm 0.65\%$ per year should be considered as an upper limit as part of this contribution could have more simply been undetected by OC remote sensing.

Spatially, the CHL trend is not uniform, with only a few areas characterized by positive values: in the Alboran Sea, Sicily Channel, and SE of Crete (Figure 4B). The rest of the basin is characterized by a negative trend with higher magnitude in the western region. This is in line with the hypothesis of decreasing nutrient availability in the upper mixed layer. In fact, on one side, the eastern basin is already characterized by a DCM-dominated phytoplankton vertical distribution structure [79] with less impact over the remote sensing observations. Furthermore, Pisano et al. [77] reported that the area most affected by the general warming trend in the Mediterranean Sea is the western sector, where the reduction in phytoplankton biomass in spring was recently documented by combining autonomous observations from BioGeoChemical-Argo floats, satellite-based, and marine ecosystem modeling [80].

As an example of the CMEMS contributions to Sustainable Development Goal (SDG) reporting, Figure 5 presents the 1998–2023 time series of the potential eutrophication (PE) for European waters based on the OC regional products. The SDG reporting for 14.1.1a Level 2 sub-indicator for European countries, which measures the index of coastal eutrophication, is carried out operationally by CMEMS in a harmonized, consistent, and integrated manner using satellite-derived CHL-a data to generate a single variable indicator [81,82]. The methodology for reporting on indicator 14.1.1a builds on the UNEP (United Nations Environment Programme) progressive monitoring approach based on both globally and nationally derived data and supplemental data to report on SDG indicators [82]. For each year, a satellite-based map of potential eutrophic areas in the European Seas is generated by comparing the per-pixel CHL-a data from the MY regional products in the reporting year with the corresponding CHL-a climatological 90th percentile (P90) established for a 20-year baseline (1998–2017) [81]. Then, the PE time series of PE potential eutrophication is calculated by performing for each year a spatial average of the PE map, weighted by pixel area over the exclusive economic zones (EEZs) of each European country [81].

(A)
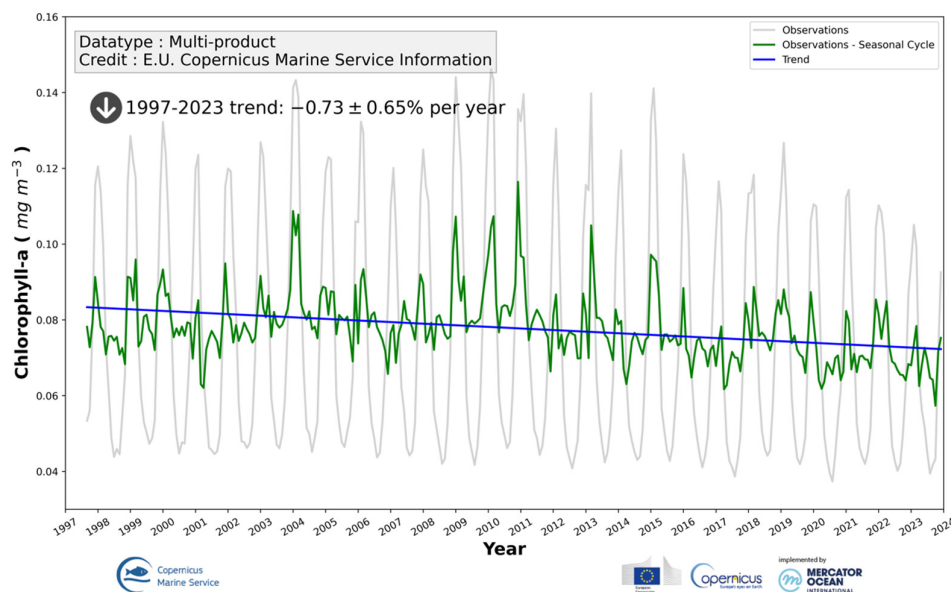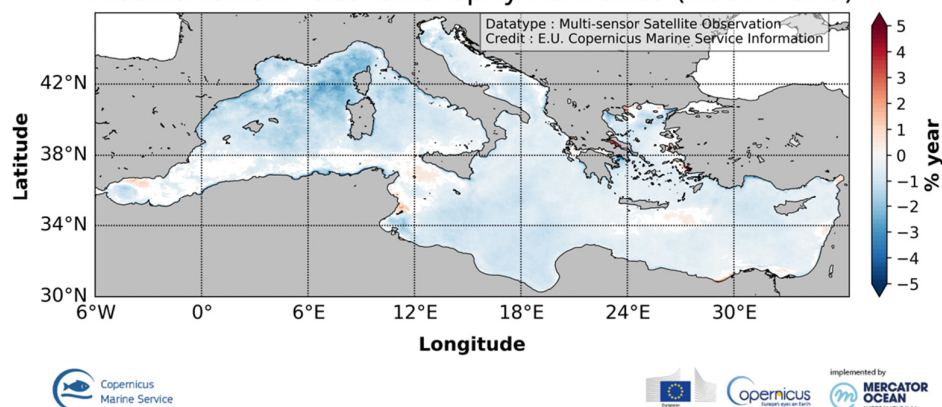
(B)

Figure 4. Mediterranean Sea satellite CHL trend over the period 1997-2023, based on the CMEMS product OCEANCOLOUR_MED_BGC_L4_MY_009_144. (**A**) Time series and linear trend of monthly regional average satellite CHL: the monthly regional average (weighted by pixel area) time series is shown in gray, with the de-seasonalized time series in green and the linear trend in blue. (**B**) Map of satellite CHL trend, expressed in % per year, with positive trends in red and negative trends in blue.

This SDG indicator has been published by Eurostat since 2021 and updated every year [83–86]; the data presented in Figure 5 are publicly available on the Eurostat data browser [87]. Due to the full reprocessing of the underlying satellite products, some of the reported values differ from those reported in previous years (e.g., [81,83]), while the overall picture remains consistent. The data computed in 2024 showed minor changes for the SDG eutrophication indicator for the Mediterranean and Black Sea, while for the Baltic countries some of the values changed significantly. The values for the Atlantic countries changed for data for 2022 due to the consolidation of the MY time series. For several countries, the SDG indicator at the EEZ level was often nil or never exceeded 1% of the EEZ area (Figure 5). Some notable deviations from the CHL climatology are evident, e.g., the high PE values observed for four Baltic countries (Lithuania, Latvia, Poland, and Sweden) in 2008 capturing the extended spring bloom reported for the central and southern Baltic Sea [45]. From 2012 onwards, all European countries yielded a eutrophication index lower than

2%, consistent with the findings based on ensemble analyses of bio-geochemical models for all European seas [45], in situ and satellite data for the Atlantic and Baltic regions (e.g., [45,88–91]), and the CMEMS OMIs as shown for the Mediterranean sea (Figure 4).
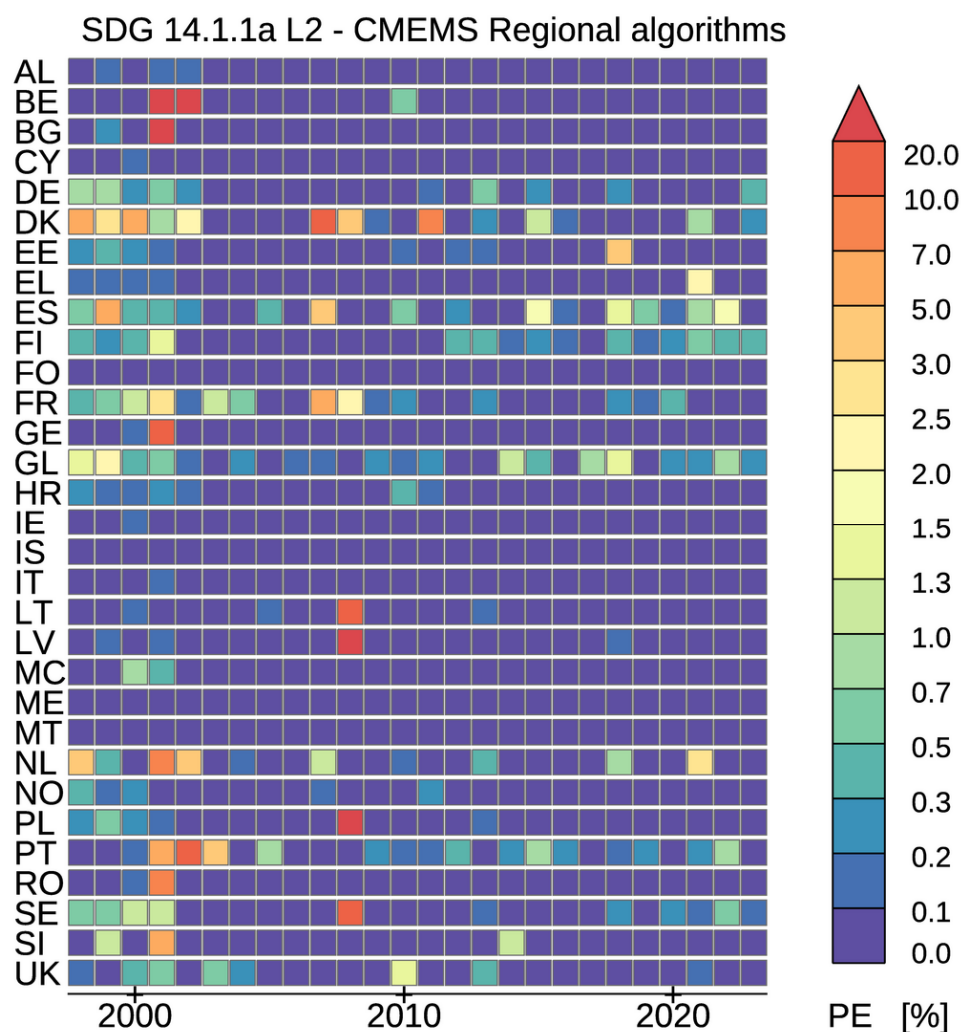
Figure 5. Time series (1998–2023) of SDG 14.1.1a Level 2 sub-indicator for European countries. The potential eutrophication values for European waters are based on CMEMS OC regional products aggregated over the EEZ for each country. AL: Albania, BE: Belgium, BG: Bulgaria, CY: Cyprus, DE: Germany, DK: Denmark, EE: Estonia, EL: Greece, ES: Spain, FI: Finland, FO: Faroe Islands, FR: France, GE: Georgia, GL: Greenland, HR: Croatia, IE: Ireland, IS: Iceland, IT: Italy, LT: Lithuania, LV: Lat- via, MC: Monaco, ME: Montenegro, MT: Malta, NL: Netherlands, NO: Norway, PL: Poland, PT: Portugal, RO: Romania, SE: Sweden, SI: Slovenia, UK: United Kingdom.

5. Future Evolutions

To ensure the state of the art of OC global and regional products, OCTAC will continue to focus on increasing the number and the accuracy of the EOVs included in the CMEMS catalogue, aiming to include most of, if not all, the EOVs that can be retrieved from OC radiometry. This will entail the uptake within the operational processing chains of algorithms and approaches developed within CMEMS and by the OC community.

In 2025–2028, the introduction of new products and/or resolution in the catalogue will be based on the uptake of outcomes from Copernicus Marine Service Evolution projects [92] and some recent internal development activities:

- Introduction of multi-resolution SPM/TUR/CHL products based on harmonized S2 and S3 products generated using multi-resolution data interpolation techniques

algorithms [93–95]. The same approach will also improve the daily L4 products for the Sentinel-2 coastal high-resolution products.

- New datasets for particulate and dissolved organic carbon will be added to the catalogue for open and coastal waters and managing the transitions between the two domains [64,65,96]. Basically, POC (particulate organic carbon) estimates result in a combination of different algorithms as a function of the optical water classes [64,96]. For the retrieval of DOC (dissolved organic carbon), the main contributor to organic carbon over open ocean water, the algorithm proposes an innovative approach considering a temporal window to account for the fate of the organic matter with a neural-net [65,96].
- Update of the phytoplankton functional types (PFTs) retrieval algorithms in the catalogue to build a more consistent time series over the OC archive based on a recalibration of the OLCI product [54,55,97].
- The generation of gap-filled R_{rs} fields using the DINEOF technique from which all subsequent biogeochemical parameters will be retrieved [98]. The introduction of gap-filled R_{rs} and IOPs datasets in L4 products will be carried out in the regional multisensor datasets for BLK, MED and BAL.

Furthermore, to enhance the accuracy of the global and regional products, new efforts will be dedicated to:

- Update ATL products based on the Copernicus-GlobColour processor [7] for the coastal waters in the North Sea to support the OSPAR (OSlo PARis convention) requirements for eutrophication assessment. This will also entail updating the OC5 algorithms for CHL and SPM retrieval [33] to be in line with the latest version of the sensor reprocessing.
- Update of the strategies to merge data from sensors with different sets of central wavelengths and spectral response functions in the processing chains. In particular, the reference sensor will be changed to OLCI.
- Extend the applicability over water types of the blended approaches for CHL retrieval in the optically complex waters in ARC, BAL, BLK, and MED, also further incorporating machine learning approaches.
- Uptake of the new L2 operational reflectance product dedicated to water applications for the Sentinel-2 MSI to be released by ESA, and regionalization of the CHL algorithms at the basin level for the Sentinel-2 MSI products to be consistent with the OLCI and multi-resolution products for each European sea.
- Full reprocessing of the MY time series to incorporate major changes to the upstream satellite data carried out by the space agencies, and the improvements listed above.

The continuous and sustained operational data stream of both observational classes currently in use (i.e., OC sensors and high-resolution imagers) is foreseen to continue beyond 2030. In 2025–2028, OCTAC will thus carry out dedicated assessments and studies to prepare the introduction of future missions and data streams in the catalogue. The assessment and uptake of the NASA PACE (Plankton, Aerosol, Cloud, Ocean Ecosystem) science mission will serve to prepare for the future exploitation of the Copernicus Sentinel 10 CHIME (Copernicus Hyperspectral Imaging Mission for the Environment) hyperspectral data currently planned for launch in 2028 and 2030 (CHIME-A and CHIME-B, Figure 3) and the Sentinel-3 Next Generation AOLCI that will be launched in the 2032–2035 time frame. After 2028, a further change in the resolutions will be the uptake of (sub-)hourly datasets for the European basins based on geostationary data by incorporating EUMETSAT MSG (Meteosat Second Generation) and MTG GEO-OC (Meteosat Second Generation Geostationary Ocean Colour Product) data-streams as well as multiple OLCI and VIIRS overpasses. This will enable to match the sub-daily time scales of the operational modelling effort within CMEMS, thus strengthening the potential for data assimilation.

References

1. von Schuckmann, K.; Le Traon, P.-Y.; Smith, N.; Pascual, A.; Djavidnia, S.; Gattuso, J.-P.; Grégoire, M.; Nolan, G.; Aaboe, S.; Aguiar, E.; et al. Copernicus Marine Service Ocean State Report 3. *J. Oper. Oceanogr.* **2019**, *12* (Suppl. S1), S1–S123. [CrossRef]
2. Von Schuckmann, K.; Le Traon, P.Y.; Menna, M.; Martellucci, R.; Notarstefano, G.; Mauri, E.; Gerin, R.; Pacciaroni, M.; Bussani, A.; Pirro, A.; et al. Copernicus Ocean State Report, Issue 6. *J. Oper. Oceanogr.* **2022**, *15* (Suppl. S1), s1–s220.
3. Letraon, P.; Ali, A.; Fanjul, E.A.; Aouf, L.; Axell, L.; Aznar, R.; Ballarotta, M.; Behrens, A.; Benkiran, M.; Bentamy, A.; et al. The Copernicus marine environmental monitoring service: Main scientific achievements and future prospects. *Mercat. Ocean. J.* **2017**, *56*, 101.
4. Le Traon, P.Y.; Reppucci, A.; Fanjul, E.A.; Aouf, L.; Behrens, A.; Belmonte, M.; Bentamy, A.; Bertino, L.; Brando, V.E.; Kreiner, M.B.; et al. From Observation to Information and Users: The Copernicus Marine Service Perspective. *Front. Mar. Sci.* **2019**, *6*, 234. [CrossRef]
5. Le Traon, P.; Abadie, V.; Ali, A.; Behrens, A.; Staneva, J.; Hieronymi, M.; Krasemann, H. The Copernicus Marine Service from 2015 to 2021: Six years of achievements. *Mercat. Ocean. J.* **2021**. [CrossRef]
6. Volpe, G.; Colella, S.; Brando, V.E.; Forneris, V.; Padula, F.L.; Di Cicco, A.; Sammartino, M.; Bracaglia, M.; Artuso, F.; Santoleri, R. Mediterranean ocean colour Level 3 operational multi-sensor processing. *Ocean Sci.* **2019**, *15*, 127–146. [CrossRef]
7. Garnesson, P.; Mangin, A.; Fanton d'Andon, O.; Demaria, J.; Bretagnon, M. The CMEMS GlobColour chlorophyll a product based on satellite observation: Multi-sensor merging and flagging strategies. *Ocean Sci.* **2019**, *15*, 819–830. [CrossRef]
8. Sathyendranath, S.; Brewin, R.; Brockmann, C.; Brotas, V.; Calton, B.; Chuprin, A.; Cipollini, P.; Couto, A.; Dingle, J.; Doerffer, R.; et al. An Ocean-Colour Time Series for Use in Climate Studies: The Experience of the Ocean-Colour Climate Change Initiative (OC-CCI). *Sensors* **2019**, *19*, 4285. [CrossRef]
9. Sathyendranath, S.; Brewin, R.J.W.; Jackson, T.; Mélin, F.; Platt, T. Ocean-colour products for climate-change studies: What are their ideal characteristics? *Remote Sens. Environ.* **2017**, *203*, 125–138. [CrossRef]
10. Dekker, A.G.; Pinnel, N.; Gege, P.; Briottet, X.; Peters, S.; Turpie, K.R.; Sterckx, S.; Costa, M.; Giardino, C.; Brando, V.E.; et al. *Feasibility Study for an Aquatic Ecosystem Earth Observing System Version 1.2*; Committee on Earth Observation Satellites (CEOS) and Commonwealth Scientific and Industrial Research Organization: Canberra, Australia, 2018.

11. GOOS. Global Ocean Observing System, Essential Ocean Variables Specification Sheet: Ocean Colour. 2018. Available online: https://www.goosocean.org/index.php?option=com_oe&task=viewDocumentRecord&docID=19959 (accessed on 22 October 2024).

12. Qin, Y.; Brando, V.E.; Dekker, A.G.; Blondeau-Patissier, D. Validity of SeaDAS Water Constituents Retrieval Algorithms in Australian Tropical Coastal Waters. *Geophys. Res. Lett.* **2007**, *34*, L21603. [CrossRef]

13. Volpe, G.; Santoleri, R.; Vellucci, V.; Ribera d'Alcalà, M.; Marullo, S.; D'Ortenzio, F. The colour of the Mediterranean Sea: Global versus regional bio-optical algorithms evaluation and implication for satellite chlorophyll estimates. *Remote Sens. Environ.* **2007**, *107*, 625–638. [CrossRef]

14. Szeto, M.; Werdell, P.J.; Moore, T.S.; Campbell, J.W. Are the world's oceans optically different? *J. Geophys. Res.* **2011**, *116*, C00H04. [CrossRef]

15. D'Alimonte, D.; Zibordi, G.; Kajiyama, T.; Berthon, J.-F. Comparison between MERIS and regional high-level products in European seas. *Remote Sens. Environ.* **2014**, *140*, 378–395. [CrossRef]

16. Beckers, J.; Rixen, M. EOF Calculations and Data Filling from Incomplete Oceanographic Datasets. *J. Atmos. Ocean.* **2003**, *20*, 1839–1856. [CrossRef]

17. Volpe, G.; Nardelli, B.B.; Colella, S.; Pisano, A.; Santoleri, R. Operational Interpolated Ocean Colour Product in the Mediterranean Sea. In *New Frontiers in Operational Oceanography*; Chassignet, E., Pascual, A., Tintoré, J., Verron, J., Eds.; CreateSpace: Scotts Valley, CA, USA, 2018; pp. 227–244.

18. Mélin, F.; Sclep, G. Band shifting for ocean color multi-spectral reflectance data. *Opt. Express* **2015**, *23*, 2262–2279. [CrossRef]

19. Jackson, T.; Sathyendranath, S.; Groom, S.; Calton, B. ESA Ocean Colour Climate Change Initiative Product User Guide for v6.0 Dataset. 2002. Available online: https://docs.pml.space/share/s/fzNSPb4aQaSDvO7xBNOCIw (accessed on 22 October 2024).

20. Steinmetz, F.; Deschamps, P.-Y.; Ramon, D. Atmospheric correction in presence of sun glint: Application to MERIS. *Opt. Express* **2011**, *19*, 9783–9800. [CrossRef]

21. Steinmetz, F.; Ramon, D. Sentinel-2 MSI and Sentinel-3 OLCI consistent ocean colour products using POLYMER. In Proceedings of the Remote Sensing of the Open and Coastal Ocean and Inland Waters, Honolulu, HI, USA, 24–25 September 2018; Volume 10778, p. 107780E.

22. EUMETSAT. Sentinel-3 OLCI L2 Report for Baseline Collection OL_L2M_003. 2021. Available online: https://user.eumetsat.int/s3/eup-strapi-media/Sentinel_3_OLCI_L2_report_for_baseline_collection_OL_L2_M_003_2_B_c8bbc6d986.pdf (accessed on 22 October 2024).

23. Tilstone, G.H.; Pardo, S.; Simis, S.G.H.; Qin, P.; Selmes, N.; Dessailly, D.; Kwiatkowska, E. Consistency between satellite ocean colour products under high coloured dissolved organic matter absorption in the baltic sea. *Remote Sens.* **2022**, *14*, 89. [CrossRef]

24. Zibordi, G.; Kwiatkowska, E.; Mélin, F.; Talone, M.; Cazzaniga, I.; Dessailly, D.; Gossn, J.I. Assessment of OLCI-A and OLCI-B radiometric data products across European seas. *Remote Sens. Environ.* **2022**, *272*, 112911. [CrossRef]

25. Vilas, L.G.; Brando, V.E.; Di Cicco, A.; Colella, S.; D'alimonte, D.; Kajiyama, T.; Attila, J.; Schroeder, T. Assessment of ocean color atmospheric correction methods and development of a regional ocean color operational dataset for the Baltic Sea based on Sentinel-3 OLCI. *Front. Mar. Sci.* **2024**, *10*, 1256990. [CrossRef]

26. Hieronymi, M.; Müller, D.; Doerffer, R. The OLCI Neural Network Swarm (ONNS): A Bio-Geo-Optical Algorithm for Open Ocean and Coastal Waters. *Front. Mar. Sci.* **2017**, *4*, 140. [CrossRef]

27. Doxani, G.; Vermote, E.; Roger, J.-C.; Gascon, F.; Adriaensen, S.; Frantz, D.; Hagolle, O.; Hollstein, A.; Kirches, G.; Li, F.; et al. Atmospheric Correction Inter-Comparison Exercise. *Remote Sens.* **2018**, *10*, 352. [CrossRef] [PubMed]

28. Doerffer, R.; Schiller, H. The MERIS Case 2 water algorithm. *Int. J. Remote Sens.* **2007**, *28*, 517–535. [CrossRef]

29. Brockmann, C.; Doerffer, R.; Peters, M.; Stelzer, K.; Embacher, S.; Ruescas, A. Evolution of the C2RCC neural network for Sentinel 2 and 3 for the retrieval of Ocean Colour products in normal and extreme optically complex waters. In Proceedings of the Living Planet Symposium, Prague, Czech Republic, 9–13 May 2016; p. 740.

30. Vanhellemont, Q. Adaptation of the dark spectrum fitting atmospheric correction for aquatic applications of the Landsat and Sentinel-2 archives. *Remote Sens. Environ.* **2019**, *225*, 175–192. [CrossRef]

31. Van der Zande, D.; Vanhellemont, Q.; Stelzer, K.; Lebreton, C.; Dille, A.; dos Santos, J.C.; Böttcher, M.; Vansteenwegen, D.; Brockmann, C. Improving operational ocean color coverage using a merged atmospheric correction approach. *Remote Sens. Ocean. Sea Ice Coast. Waters Large Water Reg.* **2023**, *12728*, 12–29. [CrossRef]

32. Hu, C.; Lee, Z.; Franz, B. Chlorophyll a algorithms for oligotrophic oceans: A novel approach based on three-band reflectance difference. *J. Geophys. Res.* **2012**, *117*, C01011. [CrossRef]

33. Gohin, F.; Druon, J.-N.; Lampert, L. A five channel chlorophyll concentration algorithm applied to SeaWiFS data processed by SeaDAS in coastal waters. *Int. J. Remote Sens.* **2002**, *23*, 1639–1661. [CrossRef]

34. Pardo, S.; Jackson, T.; Netting, J.; Calton, B.; Howey, B. Quality information document for OC TAC Products Atlantic and Arctic Observation Products. *Copernicus Marine Service*. 2022. Available online: https://catalogue.marine.copernicus.eu/documents/QUID/CMEMS-OC-QUID-009-111to114-121to124.pdf (accessed on 22 October 2024).

35. Zoffoli, M.L.; Volpe, G.; Brando, V.E.; Pitarch, J.; Gonzalez Vilas, L.; Colella, S. QUID (Quality Information Document) for Arctic Sea Observation Products. *Copernicus Marine Service*, release 2.0. 2023. Available online: https://documentation.marine.copernicus.eu/QUID/CMEMS-OC-QUID-009-121to124.pdf (accessed on 22 October 2024).

36. Goncalves-Araujo, R.; Rabe, B.; Peeken, I.; Bracher, A. High colored dissolved organic matter (CDOM) absorption in surface waters of the central-eastern Arctic Ocean: Implications for biogeochemistry and ocean color algorithms. *PLoS ONE* **2018**, *13*, e0190838. [CrossRef]

37. IOCCG. *Ocean Colour Remote Sensing in Polar Seas*; Babin, M., Arrigo, K., Bélanger, S., Forget, M.-H., Eds.; IOCCG Report Series, No. 16; International Ocean Colour Coordinating Group: Dartmouth, NS, Canada, 2015.

38. D'Alimonte, D.; Zibordi, G. Phytoplankton determination in an optically complex coastal region using a multilayer perceptron neural network. *IEEE Trans. Geosci. Remote Sens.* **2003**, *41*, 2861–2868. [CrossRef]

39. Colella, S.; Brando, V.E.; Di Cicco, A.; D'Alimonte, D.; Forneris, V.; Bracaglia, M. *Quality Information Document for Ocean Colour Mediterranean and Black Sea Observation Product Release 4.0*; Mercator Ocean International: Toulouse, France, 2024. [CrossRef]

40. Kajiyama, T.; D'Alimonte, D.; Zibordi, G. Algorithms merging for the determination of Chlorophyll-a concentration in the Black Sea. *IEEE Geosci. Remote Sens. Lett.* **2018**, *16*, 677–681. [CrossRef]

41. Zibordi, G.; Mélin, F.; Berthon, J.-F.; Talone, M. In situ autonomous optical radiometry measurements for satellite ocean color validation in the Western Black Sea. *Ocean Sci.* **2015**, *11*, 275–286. [CrossRef]

42. Kopelevich, O.; Burenkov, V.; Sheberstov, S.; Vazyulya, S.; Kravchishina, M.; Pautova, L.; Silkin, V.; Artemiev, V.; Grigoriev, A. Satellite monitoring of coccolithophore blooms in the Black Sea from ocean color data. *Remote Sens. Environ.* **2014**, *146*, 113–123. [CrossRef]

43. Zibordi, G.; Berthon, J.-F.; Mélin, F.; D'Alimonte, D. Cross-site consistent in situ measurements for satellite ocean color applications: The BiOMaP radiometric dataset. *Remote Sens. Environ.* **2011**, *115*, 2104–2115. [CrossRef]

44. D'Alimonte, D.; Zibordi, G.; Berthon, J.-F.; Canuti, E.; Kajiyama, T. Bio-Optical Algorithms for European Seas: Performance and Applicability of Neural-Net Inversion Schemes. Technical Report JRC66326, JRC-IES Scientific and Technical Reports. 2011. Available online: https://data.europa.eu/doi/10.2788/56321 (accessed on 22 October 2024).

45. Brando, V.E.; Sammartino, M.; Colella, S.; Bracaglia, M.; Di Cicco, A.; D'Alimonte, D.; Kajiyama, T.; Kaitala, S.; Attila, J. Phytoplankton Bloom Dynamics in the Baltic Sea Using a Consistently Reprocessed Time Series of Multi-Sensor Reflectance and Novel Chlorophyll-a Retrievals. *Remote Sens.* **2021**, *13*, 3071. [CrossRef]

46. Pitarch, J.; Volpe, G.; Colella, S.; Krasemann, H.; Santoleri, R. Remote sensing of chlorophyll in the Baltic Sea at basin scale from 1997 to 2012 using merged multi-sensor data. *Ocean Sci.* **2016**, *12*, 379–389. [CrossRef]

47. Lavigne, H.; Van Der Zande, D.; Ruddick, K.; Cardoso dos Santos, J.; Gohin, F.; Brotas, V.; Kratzer, S. Quality-control tests for OC4, OC5 and NIR-red satellite chlorophyll-a algorithms applied to coastal waters. *Remote Sens. Environ.* **2021**, *255*, 112237. [CrossRef]

48. O'Reilly, J.E.; Werdell, P.J. Chlorophyll algorithms for ocean color sensors-OC4, OC5 & OC6. *Remote Sens. Environ.* **2019**, *229*, 32–47. [CrossRef]

49. Gons, H.J. Optical teledetection of chlorophyll a in turbid inland waters. *Environ. Sci. Technol.* **1999**, *33*, 1127–1132. [CrossRef]

50. Gons, H.J.; Rijkeboer, M.; Ruddick, K.G. Effect of a waveband shift on chlorophyll retrieval from MERIS imagery of inland and coastal waters. *J. Plankton Res.* **2005**, *27*, 125–127. [CrossRef]

51. Brewin, R.J.W.; Sathyendranath, S.; Jackson, T.; Barlow, R.; Brotas, V.; Airs, R.; Lamont, T. Influence of light in the mixed-layer on the parameters of a three-component model of phytoplankton size class. *Remote Sens. Environ.* **2015**, *168*, 437–450. [CrossRef]

52. Brewin, R.J.W.; Ciavatta, S.; Sathyendranath, S.; Jackson, T.; Tilstone, G.; Curran, K.; Airs, R.L.; Cummings, D.; Brotas, V.; Organelli, E.; et al. Uncertainty in Ocean-Color Estimates of Chlorophyll for Phytoplankton Groups. *Front. Mar. Sci.* **2017**, *4*, 104. [CrossRef]

53. Di Cicco, A.; Sammartino, M.; Marullo, S.; Santoleri, R. Regional Empirical Algorithms for an Improved Identification of Phytoplankton Functional Types and Size Classes in the Mediterranean Sea Using Satellite Data. *Front. Mar. Sci.* **2017**, *4*, 126. [CrossRef]

54. Xi, H.; Losa, S.N.; Mangin, A.; Soppa, M.A.; Garnesson, P.; Demaria, J.; Liu, Y.; Hembise Fanton d'Andon, O.; Bracher, A. Global retrieval of phytoplankton functional types based on empirical orthogonal functions using CMEMS GlobColour merged products and further extension to OLCI data. *Remote Sens. Environ.* **2020**, *240*, 111704. [CrossRef]

55. Xi, H.; Losa, S.N.; Mangin, A.; Garnesson, P.; Bretagnon, M.; Demaria, J.; Soppa, M.A.; Hembise Fanton d'Andon, O.; Bracher, A. Global chlorophyll a concentrations of phytoplankton functional types with detailed uncertainty assessment using multi-sensor ocean color and sea surface temperature satellite products. *J. Geophys. Res. Ocean.* **2021**, *126*, e2020JC017127. [CrossRef]

56. Brando, V.E.; Gonzalez Vilas, L.; Di Cicco, A.; Sammartino, M.; Colella, S.; D'Alimonte, D.; Kajiyama, T.; Kaitala, S.; Attila, J. Ocean Colour Production Centre—Baltic Sea Observation Products (Quality Information Document, QUID). 2023. Available online: https://catalogue.marine.copernicus.eu/documents/QUID/CMEMS-OC-QUID-009-131to134.pdf (accessed on 22 October 2024).

57. Sieburth, J.M.; Smetacek, V.; Lenz, J. Pelagic ecosystem structure: Heterotrophic compartments of the plankton and their relationship to plankton size fractions. *Limnol. Oceanogr.* **1978**, *23*, 1256–1263. [CrossRef]

58. Vidussi, F.; Claustre, H.; Manca, B.B.; Luchetta, A.; Marty, J.C. Phytoplankton pigment distribution in relation to upper thermocline circulation in the eastern Mediterranean Sea during winter. *J. Geophys. Res.* **2001**, *106*, 19939–19956. [CrossRef]

59. Uitz, J.; Claustre, H.; Morel, A.; Hooker, S.B. Vertical distribution of phytoplankton communities in open ocean: An assessment based on surface chlorophyll. *J. Geophys. Res.* **2006**, *111*, C08005. [CrossRef]

60. Brewin, R.J.W.; Sathyendranath, S.; Hirata, T.; Lavender, S.J.; Barciela, R.M.; Hardman-Mountford, N.J. A three-component model of phytoplankton size class for the Atlantic Ocean. *Ecol. Model.* **2010**, *221*, 1472–1483. [CrossRef]

61. Hirata, T.; Hardman-Mountford, N.J.; Brewin, R.J.W.; Aiken, J.; Barlow, R.; Suzuki, K.; Isada, T.; Howell, E.; Hashioka, T.; Noguchi-Aita, M.; et al. Synoptic relationships between surface Chlorophyll-a and diagnostic pigments specific to phytoplankton functional types. *Biogeosciences* **2011**, *8*, 311–327. [CrossRef]

62. Lee, Z.P.; Carder, K.L.; Arnone, R.A. Deriving inherent optical properties from water color: A multiband quasi-analytical algorithm for optically deep waters. *Appl. Opt.* **2002**, *41*, 5755–5772. [CrossRef]

63. Lee, Z.P.; Carder, K.L.; Arnone, R.A. *Update of the Quasi-Analytical Algorithm (QAA_v6)*; IOCCG Software Report; International Ocean Colour Coordinating Group (IOCCG): Dartmouth, NS, Canada, 2014.

64. Jorge, D.S.F.; Loisel, H.; Jamet, C.; Dessailly, D.; Demaria, J.; Bricaud, A.; Maritorena, S.; Zhang, X.; Antoine, D.; Kutser, T.; et al. A Three-Step Semi Analytical Algorithm (3SAA) for Estimating Inherent Optical Properties over Oceanic, Coastal, and Inland Waters from Remote Sensing Reflectance. *Remote Sens. Environ.* **2021**, *263*, 112537. [CrossRef]

65. Bonelli, A.G.; Loisel, H.; Jorge, D.S.F.; Mangin, A.; d'Andon, O.F.; Vantrepotte, V. A new method to estimate the dissolved organic carbon concentration from remote sensing in the global open ocean. *Remote Sens. Environ.* **2022**, *281*, 113227. [CrossRef]

66. Maritorena, S.; Siegel, D.A. Consistent merging of satellite ocean color data sets using a bio-optical model. *Remote Sens. Environ.* **2005**, *94*, 429–440. [CrossRef]

67. Antoine, D.; Morel, A. Oceanic primary production: 1. Adaptation of a spectral light-photosynthesis model in view of application to satellite chlorophyll observations. *Glob. Biogeochem. Cycles* **1996**, *10*, 43–55. [CrossRef]

68. Frouin, R.; Franz, B.A.; Werdell, P.J. The SeaWiFS PAR product. In *Algorithm Updates for the Fourth SeaWiFS Data Reprocessing*; Hooker, S.B., Firestone, E.R., Eds.; NASA/TM-2003-206892; NASA Goddard Space Flight Center: Greenbelt, MD, USA, 2003; Volume 22, pp. 46–50.

69. CMEMS. *Global Ocean Physics Reanalysis GLORYS12V1 Product*; CMEMS: Ramonville-Saint-Agne, France, 2022. [CrossRef]

70. Morel, A. Light and marine photosynthesis: A spectral model with geochemical and climatological implications. *Prog. Oceanogr.* **1991**, *26*, 263–306. [CrossRef]

71. Tanré, D.; Herman, M.; Deschamps, P.Y.; De Leffe, A. Atmospheric modeling for space measurements of ground reflectances, including bidirectional properties. *Appl. Opt.* **1979**, *18*, 3587–3594. [CrossRef]

72. Morel, A.; Berthon, J.F. Surface pigments, algal biomass profiles, and potential production of the euphotic layer: Relationships reinvestigated in view of remote-sensing applications. *Limnol. Oceanogr.* **1989**, *34*, 1545–1562. [CrossRef]

73. Gregg, W.W.; Casey, N.W. Skill assessment of a spectral ocean-atmosphere radiative model. *J. Mar. Syst.* **2009**, *76*, 49–63. [CrossRef]

74. Hernandez, F.; Smith, G.; Baetens, K.; Cossarini, G.; Garcia-Hermosa, I.; Drévillon, M.; Maksymczuk, J.; Melet, A.; Régnier, C.; Schuckmann, K.V. Measuring performances, skill and accuracy in operational oceanography: New challenges and approaches. In *New Frontiers in Operational Oceanography*; Chassignet, E., Pascual, A., Tintoré, J., Verron, J., Eds.; GODAE OceanView: Mallorca, Spain, 2018; pp. 759–796. [CrossRef]

75. Concha, J.A.; Bracaglia, M.; Brando, V.E. Assessing the Influence of Different Validation Protocols on Ocean Colour Match-up Analyses. *Remote Sens. Environ.* **2021**, *259*, 112415. [CrossRef]

76. Valente, A.; Sathyendranath, S.; Brotas, V.; Groom, S.; Grant, M.; Jackson, T.; Chuprin, A.; Taberner, M.; Airs, R.; Antoine, D.; et al. A compilation of global bio-optical in situ data for ocean colour satellite applications–version three. *Earth Syst. Sci. Data* **2022**, *14*, 5737–5770. [CrossRef]

77. Pisano, A.; Marullo, S.; Artale, V.; Falcini, F.; Yang, C.; Leonelli, F.E.; Santoleri, R.; Buongiorno Nardelli, B. New Evidence of Mediterranean Climate Change and Variability from Sea Surface Temperature Observations. *Remote Sens.* **2020**, *12*, 132. [CrossRef]

78. Marullo, S.; Serva, F.; Iacono, R.; Napolitano, E.; di Sarra, A.; Meloni, D.; Monteleone, F.; Sferlazzo, D.; De Silvestri, L.; de Toma, V.; et al. Record-breaking persistence of the 2022/23 marine heatwave in the Mediterranean Sea. *Environ. Res. Lett.* **2023**, *18*, 114041. [CrossRef]

79. Volpe, G.; Nardelli, B.B.; Cipollini, P.; Santoleri, R.; Robinson, I.S. Seasonal to interannual phytoplankton response to physical processes in the Mediterranean Sea from satellite observations. *Remote Sens. Environ.* **2012**, *117*, 223–235. [CrossRef]

80. Li, M.; Organelli, E.; Serva, F.; Bellacicco, M.; Landolfi, A.; Pisano, A.; Marullo, S.; Shen, F.; Mignot, A.; van Gennip, S.; et al. Phytoplankton spring bloom inhibited by marine heatwaves in the North-Western Mediterranean Sea. *Geophys. Res. Lett.* **2024**, *51*, e2024GL109141. [CrossRef]

81. Brando, V.E.; Pardo, S.; Sathyendranath, S.; Howey, B.; Land, P.; Jackson, T.; Santoleri, R.; Sammartino, M.; Colella, S.; von Schuckmann, K.; et al. Potential eutrophication of European waters using satellite derived chlorophyll following the UN Sustainable Development Goal 14 framework. *J. Oper. Oceanogr.* **2022**, *15* (Suppl. S1), s83–s91. [CrossRef]

82. UNEP. *Understanding the State of the Ocean: A global Manual on Measuring SDG 14.1.1, SDG 14.2.1 and SDG 14.5.1*; UNEP: Nairobi, Kenya, 2021.

83. Eurostat. *Sustainable Development in the European Union. Monitoring Report on Progress Towards the SDGs in an EU Context (Cat. No: KS-03-21-096-EN-N)*; Eurostat: Luxembourg, 2021; ISBN 978-92-76-30698-6. [CrossRef]

84. Eurostat. *Sustainable Development in the European Union. Monitoring Report on Progress Towards the SDGs in an EU Context—2022 Edition (KS-09-22-019-EN-N)*; Eurostat: Luxembourg, 2022. [CrossRef]

85. Eurostat. *Sustainable Development in the European Union. Monitoring Report on Progress Towards the SDGs in an EU Context—2023 Edition (KS-04-23-184-EN-N)*; Eurostat: Luxembourg, 2023. [CrossRef]

86. Eurostat. *Sustainable Development in the European Union. Monitoring Report on Progress Towards the SDGs in an EU Context—2024 Edition (Cat: KS-05-24-071-EN-N)*; Eurostat: Luxembourg, 2024. [CrossRef]

87. Eurostat. *Marine Waters Affected by Eutrophication. Eurostat Data Browser—Online Data Code: Sdg_14_60 (Last Accessed on 22 October 2024)*; Eurostat: Luxembourg, 2024. [CrossRef]

88. Friedland, R.; Macias, D.M.; Cossarini, G.; Daewel, U.; Estournel, C.; Garcia-Gorriz, E.; Grizzetti, B.; Grégoire, M.; Gustafson, B.; Kalaroni, S.; et al. Effects of nutrient management scenarios on marine eutrophication indicators: A Pan-European, multi-model assessment in support of the Marine Strategy Framework Directive. *Front. Mar. Sci.* **2021**, *8*, 596126. [CrossRef]

89. Axe, P.; Clausen, U.; Leujak, W.; Malcolm, S.; Ruiter, H.; Prins, T.; Harvey, E.T.; OSPAR Coimmission. *Eutrophication Status of the OSPAR Maritime Area. Third Integrated Report on the Eutrophication Status of the OSPAR Maritime Area*; OSPAR Commission: London, UK, 2017; p. 165. ISBN 978-1-911458-34-0.

90. Gohin, F.; Van der Zande, D.; Tilstone, G.; Eleveld, M.A.; Lefebvre, A.; Andrieux-Loyer, F.; Blauw, A.N.; Bryère, P.; Devreker, D.; Garnesson, P.; et al. Twenty years of satellite and in situ observations of surface chlorophyll-a from the northern Bay of Biscay to the eastern English Channel. Is the water quality improving? *Remote Sens. Environ.* **2019**, *233*, 111343. [CrossRef]

91. Prins, T.; Enserink, L. Concentrations of Chlorophyll-a in the Greater North Sea, Celtic Seas and Bay of Biscay and Iberian Coast. In *The 2023 Quality Status Report for the Northeast Atlantic*; OSPAR Commission: London, UK, 2023; Available online: https://oap.ospar.org/en/ospar-assessments/quality-status-reports/qsr-2023/indicator-assessments/chl-a-concentrations (accessed on 22 October 2024).

92. CMEMS. *Copernicus Marine Service Evolution Projects*; CMEMS: Ramonville-Saint-Agne, France, 2024; Available online: https://marine.copernicus.eu/about/research-development-projects (accessed on 24 October 2024).

93. Alvera-Azcárate, A.; Van der Zande, D.; Barth, A.; Dille, A.; Massant, J.; Beckers, J.-M. Generation of super-resolution gap-free ocean colour satellite products using DINEOF. *EGUsphere* **2024**. [CrossRef]

94. Alvera-Azcárate, A.; van der Zande, D.V.; Barth, A.; dos Santos, J.F.C.; Troupin, C.; Beckers, J.-M. Detection of shadows in high spatial resolution ocean satellite data using DINEOF. *Remote Sens. Environ.* **2021**, *253*, 112229. [CrossRef]

95. Alvera-Azcárate, A.; van der Zande, D.V.; Barth, A.; Troupin, C.; Martin, S.; Beckers, J.-M. Analysis of 23 Years of Daily Cloud-Free Chlorophyll and Suspended Particulate Matter in the Greater North Sea. *Front. Mar. Sci.* **2021**, *8*, 707632. [CrossRef]

96. Loisel, H.; Duforêt-Gaurier, L.; Tran, T.K.; Schaffer Ferreira Jorge, D.; Steinmetz, F.; Mangin, A.; Bretagnon, M.; Hembise Fanton d'Andon, O. Characterization of the organic vs. inorganic fraction of suspended particulate matter in coastal waters based on ocean color radiometry remote sensing. In *7th Edition of the Copernicus Ocean State Report (OSR7)*; von Schuckmann, K., Moreira, L., Le Traon, P.-Y., Grégoire, M., Marcos, M., Staneva, J., Brasseur, P., Garric, G., Lionello, P., Karstensen, J., et al., Eds.; Copernicus Publications, State Planet: Göttingen, Germany, 2023; Volume 1-osr7, p. 11. [CrossRef]

97. Xi, H.; Bretagnon, M.; Losa, S.N.; Brotas, V.; Gomes, M.; Peeken, I.; Alvarado, L.; Mangin, A.; Bracher, A. Satellite monitoring of surface phytoplankton functional types in the Atlantic Ocean over 20 years (2002–2021). *State Planet* **2023**, *1*, 5.

98. Marchese, C.; Colella, S.; Brando, V.E.; Zoffoli, M.L.; Volpe, G. Towards accurate L4 Ocean Colour products: Interpolating Remote Sensing Reflectance via DINEOF. *Int. J. Appl. Earth Obs. Geoinf.* **2024**, *135*, 104270. [CrossRef]